

Article

Transparent, High-Strength, and Antimicrobial Polyvinyl Alcohol/Boric Acid/Poly Hexamethylene Guanidine Hydrochloride Films

Shaotian Zhang, Dafu Wei *, Xiang Xu and Yong Guan *

School of Materials Science and Engineering, East China University of Science and Technology, Shanghai 200237, China; 17717919604@163.com (S.Z.); xiangxu@ecust.edu.cn (X.X.)

* Correspondence: dfwei@ecust.edu.cn (D.W.); yguan@ecust.edu.cn (Y.G.)

Abstract: It is still crucial to improve the mechanical characteristics of polyvinyl alcohol (PVA) films without resorting to chemical cross-linking. In this study, boric acid (BA) was used to enhance the mechanical characteristics of PVA films while maintaining their excellent transparency and biodegradability. The hydrogen bond interaction between PVA and BA resulted in a 70% increase in tensile strength (from 48.5 to 82.1 MPa) and a 46% increase in elongation at break (from 150 to 220%). To introduce antibacterial properties, polyhexamethylene guanidine hydrochloride (PHMG) was incorporated into PVA/BA composite films resulting in PVA/BA/PHMG composite films. The PVA/BA/PHMG films exhibited 99.99% bacterial inhibition against *Escherichia coli* and *Staphylococcus aureus* with negligible leaching of PHMG. The PVA/BA/PHMG films maintained a tensile strength of 75.3 MPa and an elongation at a break of 208%. These improved mechanical and antimicrobial properties make PVA/BA and PVA/BA/PHMG films promising for applications in food and medicinal packaging.

Keywords: PVA films; boric acid; polyhexamethylene guanidine hydrochloride; mechanical properties; antimicrobial properties



Citation: Zhang, S.; Wei, D.; Xu, X.; Guan, Y. Transparent, High-Strength, and Antimicrobial Polyvinyl Alcohol/Boric Acid/Poly Hexamethylene Guanidine Hydrochloride Films. *Coatings* **2023**, *13*, 1115. <https://doi.org/10.3390/coatings13061115>

Academic Editor: Julie M. Goddard

Received: 17 May 2023

Revised: 10 June 2023

Accepted: 14 June 2023

Published: 17 June 2023



Copyright: © 2023 by the authors. Licensee MDPI, Basel, Switzerland. This article is an open access article distributed under the terms and conditions of the Creative Commons Attribution (CC BY) license (<https://creativecommons.org/licenses/by/4.0/>).

1. Introduction

In recent years, there has been an increasing interest among researchers of various sciences in polymers that exhibit excellent biocompatibility, biodegradability, and potential for modification [1,2]. Polyvinyl alcohol (PVA) has been widely used in films [3–5], hydrogels [6–9], fibers [10–12], nanobody-based beads [13], and other fields due to its good mechanical properties, oxygen barrier [14–16], optical transparency, biocompatibility, and biodegradability. Water-soluble PVA film is an emerging green and environmentally friendly material that is non-polluting, non-toxic, and suitable for food and pharmaceutical packaging [17–20].

A crucial need is for the PVA film to have excellent mechanical characteristics. The mechanical characteristics of PVA film were typically enhanced by physical mixing and cross-linking modification. One of the key techniques for producing high-performance polymer compounds is physical mixing [21,22]. The additives, such as graphene oxide (GO) [22], silver nanoparticles [23], and silica [24], might interact with the hydroxyl group on PVA. Zhu et al. [22] combined GO and single-walled carbon nanotubes with PVA films to boost their tensile strength from 34.6 to 62.8 MPa. Fan et al. [23] found that adding silver-loaded nano-cellulose enhanced the tensile strength of PVA films, and the nanocomposite films displayed reduced moisture absorption and efficient antibacterial properties. The cross-linking of PVA films includes radiation cross-linking and chemical cross-linking [25,26]. Irradiation cross-linking can form new linkage bonds via the free radicals generated by radiation. In order to create three-dimensional porous foam structures, Sabourian et al. [25] exposed PVA/polyvinylpyrrolidone mixes to γ rays. This enhanced

the tensile strength of PVA foams from 0.43 to 0.54 MPa and the elongation at break from 30 to 205 percent. Macromolecular chains are connected to create a network structure using chemical cross-linking. According to Chen et al. [26] the PVA that had been cross-linked with sodium borate under these circumstances increased in tensile strength (from 23.3 to 66.5 MPa) but decreased in elongation at break (from 60% to 30%), and its degradable characteristics deteriorated. The antimicrobial properties of PVA films are also in great demand. Blending [27–29] and graft modification of PVA [30] are the common methods to obtain antimicrobial PVA films.

A quick and effective way to achieve antibacterial characteristics is by physical mixing. Antimicrobial PVA was created using a variety of antimicrobial substances, including chitosan [27,28], TiO₂ [29], and silver [30]. Growing interest is being paid to TiO₂ and other photo-catalytical antibacterial substances with potent bactericidal properties. Ma et al. [29] created a TiO₂/N-halamine nanoparticles/PVA composite film that, in 30 min, rendered 99.97% of *S. aureus* and 100% of *E. coli* inactive. The antibacterial composite PVA films also showed outstanding storage stability, regeneration potential, and UV light stability. Physical blending has the drawback of causing the blended antimicrobial ingredient to seep from the modified film, reducing the antimicrobial characteristics' longevity. Antimicrobial agent leaching may be reduced by graft modification. Mei et al.'s in situ green synthesis approach was used to create N-halamine compound-grafted PVA electrospun nanofibrous membranes with rechargeable antibacterial activity. In order to reduce the amount of *E. coli* by 6 log CFU in only one minute, the chlorinated dimethylol-5,5-dimethylhydantoin (DMDMH)-grafted PVA nanofiber film shows a combination of qualities, including long-term durability and great mechanical strength. However, processing and the complexity of incompletely reacted monomers continue to be issues. As a reinforcing agent in this study, boric acid (BA), a substance with water solubility, non-toxicity, and bacteriostatic qualities, was selected. Because of its aqueous solubility, wide range, and superior antibacterial capabilities, polyhexamethylene guanidine (PHMG) was selected as the antimicrobial agent. To create PVA/BA films with outstanding mechanical characteristics, PVA solution, and BA solution were combined, then dried. While maintaining a similar elongation at break to pure PVA films, the PVA film's tensile strength was increased thanks to the strong hydrogen bonds between BA and PVA. Additionally, PVA, BA, and PHMG solutions were combined to create PVA, BA, and PHMG films that, thanks to hydrogen bonds, had excellent mechanical properties and were transparent, non-leaching, and antibacterial. It is anticipated that PVA/BA and PVA/BA/PHMG films will be used in the domains of food and pharmaceutical packaging [31–33].

To the best of our knowledge, there has not been investigated the potential of the PVA and PVA–BA blends with or without the addition of PHMG as the active agent and their antibacterial and physicochemical properties as a natural preservative in coatings. This work studied the effect of both BA and PHMG (two antibacterial components) on the physicochemical and biological properties of PVA-based materials. The obtained results allowed for an evaluation of a likely increase or decrease in the antibacterial effect of PVA-based materials modified with both biologically active compounds.

2. Experiment

2.1. Materials and Methods

PVA with an average molecular weight of 73,000–78,000 (g/mol) and a hydrolysis degree of 98–99% was purchased from Shanghai Titan Technology Co. (Shanghai, China). The boric acid (AR ≥ 99.5 percent) was provided by Shanghai Aladdin Biotechnology Co. (Shanghai, China). The PHMG with a molecular weight of 740 Da was synthesized using the method described by Wei et al., 2009 [34] (as measured by ESI-TOF-MS).

2.2. Preparation of PVA/BA Films and PVA/BA/PHMG Films

A 10-weight percent PVA aqueous solution was made by mixing 50 g of PVA with 450 g of deionized (DI) water. The mixture was then agitated at 95 °C for four hours. The boric

acid (BA) was mixed with the DI water for an hour at room temperature using magnetic stirring. The mixed solution, which was then cast onto glass Petri dishes, defoamed, and dried to make PVA/BA films, was made by mixing PVA and BA solutions in a variety of mass ratios. Films having a PVA/BA concentration of 1.0 wt% BA were recorded as PVA-1.0 wt%, and so on. Next, a group of the dried films was assembled and put to the test. At room temperature, PHMG was dissolved in DI water using magnetic stirring for 4 h. The three solutions, PVA, BA, and PHMG, were combined in various mass ratios, agitated for one hour, then cast on glass Petri plates, and maintained at room temperature. PVA/BA/PHMG-0.1 wt% was the designation for the PVA/BA/PHMG film that included 0.5 wt% BA and 0.1 wt% PHMG, and so on. The dried films were then gathered and examined [22].

2.3. Characterization

2.3.1. Fourier-Transform Infrared Spectroscopy (FTIR)

In order to evaluate the functional groups on the surface, PVA films were scanned using a Nicolet 5700 spectrometer in attenuated total reflectance (ATR) mode across the 4000–400 cm^{-1} wavenumber range following the method described by Abedinia et al. [35].

2.3.2. Water Solubility (WS)

To calculate the WS, the specimens were initially cut into 5 cm \times 5 cm strips. The films were then dried at 60 $^{\circ}\text{C}$ for 24 h to determine their initial dry matter (M_i). The samples were then baked at 20 $^{\circ}\text{C}$ for 28 days in 250 mL of DI water. The samples were dried again for 24 h at 60 $^{\circ}\text{C}$ to reach their final dry weight (M_f). Equation (1) was used to calculate the WS%. The samples were examined three times, and the findings were represented as WS% [35].

$$\text{WS (\%)} = \frac{M_i - M_f}{M_i} \quad (1)$$

2.3.3. Light Transmission

The quantity of light that went through the films in the range of 200–800 nm was measured using an ultraviolet-visible (UV-vis) spectrophotometer (Lambda 950, Perkin Elmer, Waltham, MA, USA). The film samples were cut into 4 cm \times 1 cm strips and placed into cuvettes. An empty cuvette was used as a reference. The transparency of the film was calculated with the following Equation (2):

$$\text{Transparency} = -\log T/x \quad (2)$$

where T is the transmission (%) at 600 nm, and x is the thickness of the film (cm).

2.3.4. X-ray Diffraction (XRD)

Wide-angle XRD was used to analyze the crystalline structures of PVA films using a rotating anode X-ray powder diffractometer (18 KW/D/max2550 VB/PC, Rigaku Corporation, Tokyo, Japan) with Cu $K\alpha$ radiation ($\lambda = 1.542 \text{ \AA}$) at a voltage of 30 kV and current of 15 mA. Film samples were cut into 3 cm \times 3 cm and placed on the glass slides, then secured with tapes before being placed in the diffractometer chamber for measurement. The angle diffraction ranges and scanning times were set between $2\theta = 1 - 60^{\circ}$ and 2° per minute, respectively.

2.3.5. Thermogravimetric Analysis (TGA)

The thermal stability of the PVA sheets was evaluated using TGA (STA409PC, NET-ZSCH, Selb, Germany). All experiments used samples weighing around 10 mg and were conducted at temperatures ranging from 20 to 600 $^{\circ}\text{C}$ at a rate of 10 $^{\circ}\text{C}/\text{min}$ under a N_2 (purity $\geq 99.999\%$) flow rate of 50 mL/min.

2.3.6. Differential Scanning Calorimeter (DSC)

The thermal properties of the PVA/BA films were evaluated using DSC (Perkin Elmer, Waltham, MA, USA). The sample pan for the DSC apparatus received a sample of about 5 mg. An empty aluminum pan was used as a reference. While being scanned from 0 to 250 °C, samples were heated at a rate of 5 °C/min.

2.3.7. Morphology Observations by Scanning Electron Microscopy (SEM)

The morphology of the films was examined using a SEM (Hitachi S-3400N, Tokyo, Japan) at an accelerating voltage of 15 kV. The samples were coated with gold prior to inspection. Scans were performed by considering the magnification of 4000× [35].

2.3.8. Mechanical Properties

PVA films' tensile strength and elongation at break were measured using a universal electrical testing apparatus at a speed of 50 mm/min and a temperature of 23 ± 2 °C. (CMT-2203, MTS, Eden Prairie, MN, USA). Each sample had a gauge length of 25 mm. On each sample, at least five tests were run, and the average result was calculated [35].

2.3.9. Antimicrobial Tests

The bactericidal properties of PVA films were assessed using the shaking flask method [32] and the ring diffusion technique [33].

The flask-shaking method is a kind of quantitative test. Before being further diluted to 10⁵ CFU/mL, *Staphylococcus aureus* (*S. aureus*) and *Escherichia coli* (*E. coli*) were cultured in nutritive broth at 37 °C for 24 h. Then, 0.10 g of the sample and 5 mL of the bacterial culture (10⁵ CFU/mL) were combined, and they were shaken for an hour at 250 rpm at 37 °C. Following some shaking, this culture was diluted repeatedly, and 0.1 mL of it was then seeded on LB agar in a Petri dish. After the dishes had been incubated at 37 °C for 24 h, the colonies were counted. The inhibition rate of cell growth was calculated from Equation (3):

$$\text{Growth inhibition rate} = (A - B)/A \times 100\% \quad (3)$$

where A and B stand for the number of bacterial colonies discovered in the control and composite film samples, respectively. The average values of the inhibition rates were calculated after three measurements of each sample were taken.

The ring diffusion test was used to explain the leaching property. The bacterial culture medium was nutrient agar. Agar plates were inoculated with 0.1 mL solutions of *E. coli* or *S. aureus* containing 10⁸ CFU/mL. Circular pieces of film with a diameter of 0.5 cm were placed on the agar plates. Following a 24 h incubator incubation period at 37 °C, the inhibition zones' widths were measured. On each test, duplicate tests were conducted.

2.3.10. Leaching Tests

A 1 g PVA film was soaked in 50 g DI water for seven days at different temperatures. Then, using an ultraviolet (UV) spectrophotometer (Lambda 950, Perkin Elmer, Waltham, MA, USA) operating in the 190–400 nm wavelength range, the PHMG leaching rates were determined from the soaking solution. The calibration Equation (4) [36,37] of the absorbance at 192 nm of PHMG is as follows:

$$A_{192} = 0.06107 + 0.06805C_{\text{PHMG}} \quad (4)$$

where A_{192} represents the absorbance at 192 nm, C_{PHMG} represents the concentration of PHMG in µg/mL. The leaching rate was calculated by the following Equation (5):

$$\text{Leaching rate} = C_{\text{PHMG}}V_W/W_A \times 100\% \quad (5)$$

where W_A is the weight (g) of incorporated PHMG, V_W is the volume (mL) of the soaked solution, and C_{PHMG} represents the concentration of PHMG in µg/mL of soaked solution.

2.4. Gaussian Simulation

The intra- and intermolecular hydrogen bonding in the PVA/BA system was evaluated using Gaussian simulation. Gaussian 09W is the Gaussian variation. The structural optimization approach is b3lyp/6-31g**, and the energy of the H-bond is then determined using def2Tzvpp/m062x based on the electron density of the bond-critical point. The equation is as follows:

$$E_{HB} = -223.08 \times \rho(BCP) + 0.7423 \tag{6}$$

where $\rho(BCP)$ is electron density at bond-critical points, E_{HB} is the energy of the H-bond [38]. The bond-critical point is a positive saddle point on the potential energy surface.

2.5. Statistical Analysis

All the tests on each sample were performed in triplicate. Data were analyzed using one-way analysis of variance (ANOVA) in SPSS 22.0 (Chicago, IL, USA). Significant differences in the mean values were examined using Duncan’s multiple range test at $p < 0.05$. The results are expressed as mean and standard deviation.

3. Results and Discussion

3.1. Transparency and UV(Ultraviolet–Visible) Absorption of Films

High optical transparency is a crucial characteristic of PVA films. The transmittance-wavelength curves from the UV-vis spectrophotometer used to evaluate the transparency of PVA/BA films are shown in Figure 1. In the 250–800 nm range, pure PVA films show excellent transparency, especially in the visible region where the transmittance approaches 91%. The PVA and BA films both have equivalent optical transparency. The great compatibility of PVA and BA, which is most likely brought on by their strong H-bond interaction, is what accounts for the high transparency.

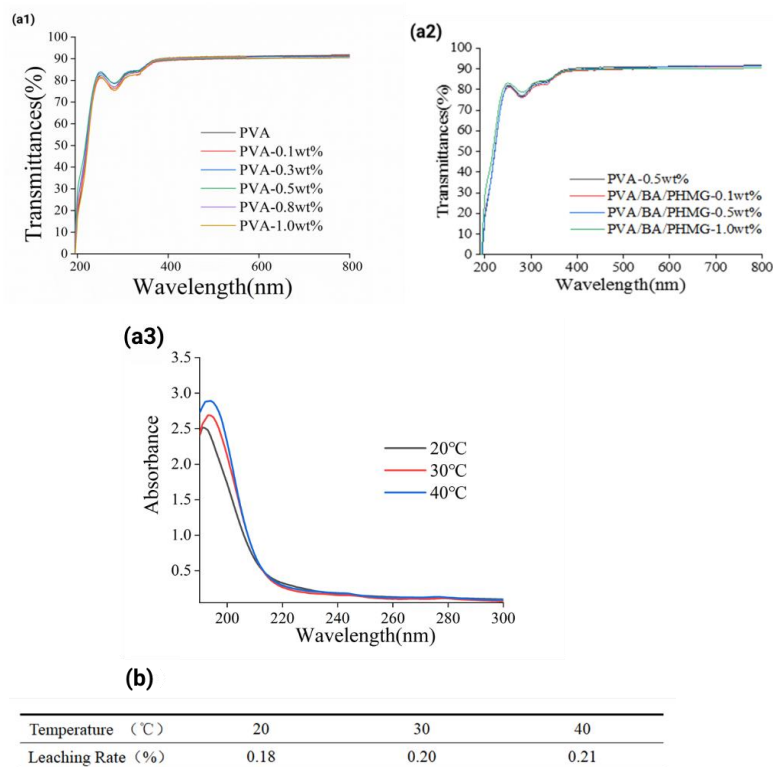


Figure 1. (a1–a3) UV-vis curves (200–800 nm) of PVA, PVA/BA (a1), and PVA/BA/PHMG (a2) films and the UV absorption spectra of soaking solution of PVA/BA/PHMG-1 wt% samples after immersion in deionized water for seven days (a3). (b) The dissolution rates of PVA/BA/PHMG-1 wt% samples at different temperatures immersion.

Leaching tests revealed that the UV absorption spectra of the PVA/BA/PHMG-1 wt% film soaking solution after seven days of immersion are shown in Figure 1b. The breakdown rate of PHMG as determined from the UV absorption spectra is shown in the attached table to Figure 1(a3). The strength at 192 nm rose with the rise in immersion temperature, and the absorption peak at that wavelength is attributed to PHMG. At 20 °C, 30 °C, and 40 °C of immersion temperature, the dissolving rates of PVA/BA/PHMG-1 wt% films were 0.18 percent, 0.20 percent, and 0.21 percent, respectively. The PVA/BA/PHMG-1 wt% film's low PHMG dissolution rate suggested that PHMG had been integrated with the PVA matrix. Guo et al. [32] also obtained similar results after treating PVA with PHMB to increase the antibacterial performance of cotton dressings with ultraviolet radiation for seven days and were able to maintain the antibacterial rate of 99.99%.

3.2. Mechanical and Water Solubility Properties of Films

The pure PVA films had tensile strength and elongation at a break of 48.5 MPa and 150.3%, respectively (Figure 2). As more BA was added up to 0.5 weight percent, the tensile strength of PVA/BA films increased, reaching 82.1 MPa for PVA-0.5 wt percent (Figure 2a). However, as the amount of BA was increased above 0.5 wt%, the tensile strength of PVA/BA films decreased, reaching 66.7 MPa for PVA-1.0 wt%. The maximum tensile strength for PVA-0.5 wt% may have indicated that the H-bond networks and physical cross-linking sites at 0.5 wt% BA may be at an ideal state. The elongation at break is shown in Figure 2b. As the amount of BA within 0.5 weight percent increased, the PVA/BA film's elongation at break increased. However, the elongation at break of the PVA/BA films decreased as the amount of BA increased above 0.5 wt percent. The change in elongation at break should also be connected to the H-bonds.

The PVA-0.5 wt% film had a tensile strength of 81.2 MPa and an elongation at a break of 220 percent. With the addition of PHMG, PVA/BA/PHMG-0.1 wt% film had a tensile strength of 75.3 MPa and an elongation at a break of 208 percent. The reduction in its mechanical properties may be due to the inclusion of PHMG, which altered the well-ordered structure between PVA and BA.

The water solubility of the films is given in the table below, Figure 2. The PVA-1.0 wt%BA film was barely soluble, whereas the pure PVA and BCPVA-0.1 films were entirely soluble. At greater BA levels, the water solubility rapidly decreased. The possibility of these hydroxyl groups forming bonds with water molecules was reduced due to the cross-linking between BA and the hydroxyl groups of PVA. For a crosslinker inserted into a polymer, similar outcomes were reported [32].

3.3. H-Bond Interaction between PVA and BA

The IR spectra of PVA and PVA/BA films were used to analyze the H-bond interaction between PVA and BA. During the formation of an H-bond, the density of the electron cloud is averaged, which reduces the frequency of stretching vibrations. Pure PVA exhibits a strong and wide absorption band at 3000–3600 cm^{-1} focused at 3264 cm^{-1} due to the stretching vibration of hydroxyl groups (O-H), including the massive H-bond (free hydroxyls is usually only observed at 3620 cm^{-1}) Figure 3. Two nearby substantial absorption peaks at 2937 cm^{-1} and 2907 cm^{-1} were seen because of the methylene's stretching vibration. The absorption peak for BA at 3180 cm^{-1} is assumed to be caused by stretching vibrations of the O-H group. For PVA/BA films, the BA absorption peak at 3180 cm^{-1} disappeared. The peak of the O-H group is moved from 3264 cm^{-1} for pristine PVA film to 3241 cm^{-1} for PVA-0.1 wt%, 3240 cm^{-1} for PVA-0.3 wt%, 3239 cm^{-1} for PVA-0.5 wt%, 3240 cm^{-1} for PVA-0.8 wt%, and 3243 cm^{-1} for PVA-1.0 wt%. The altered O-H group absorption peak, however, does not demonstrate an H-bond between PVA and BA.

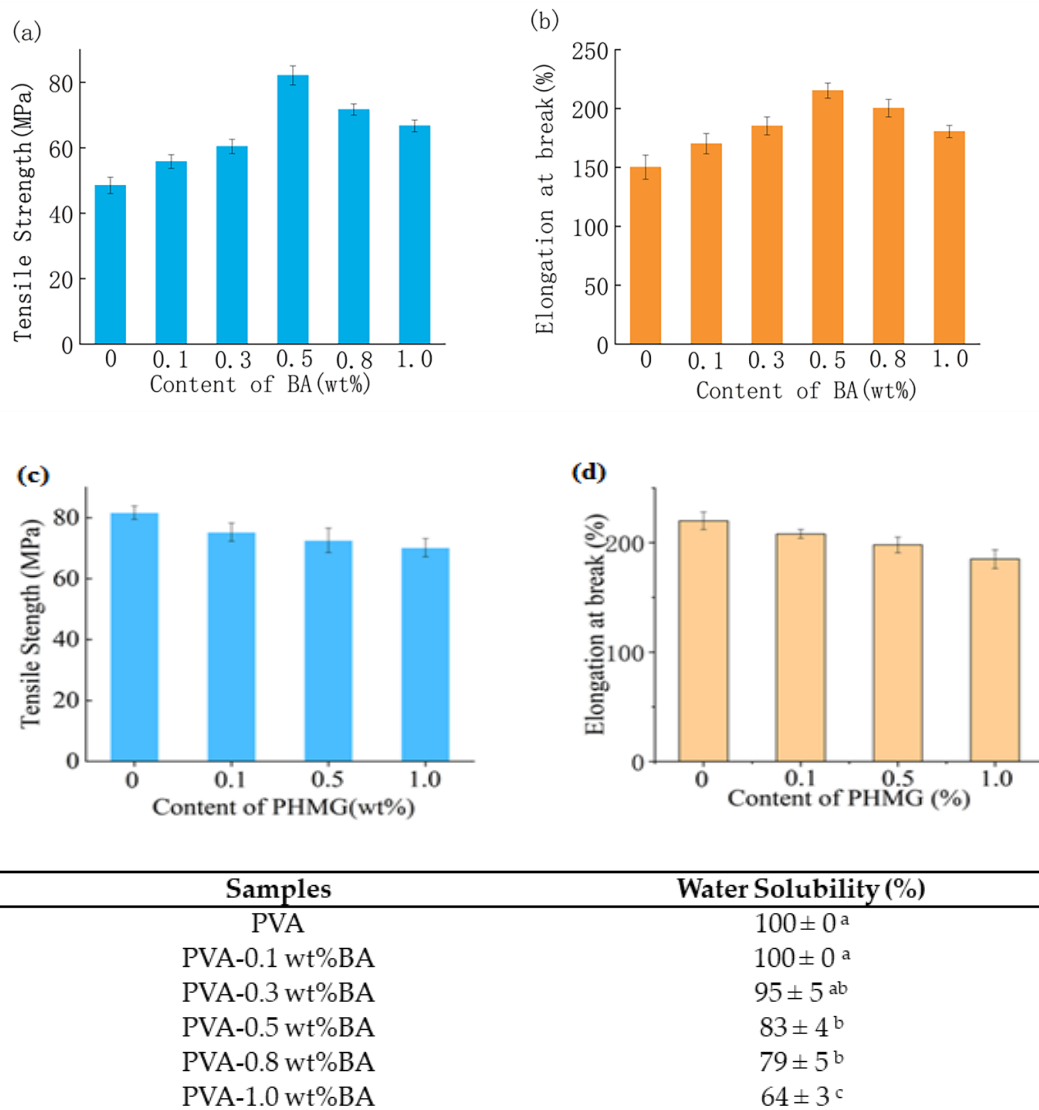


Figure 2. Mechanical properties of PVA and PVA/BA films. (a) Tensile strength, (b) elongation at break; PVA/BA and PVA/BA/PHMG films, (c) tensile strength, (d) elongation at break and stability of PVA films during 28 days in DI water 15 °C (Significant difference analysis abc letter notation).

Gaussian simulation may provide the theoretical evidence of the H-bond. The stronger the H-bond, the closer the relative distance between the atoms. In order to reduce the difficulty in the simulation, 1,3-propanediol was chosen as the model compound of PVA in the Gaussian simulation. In electrically neutral systems, the energy of intermolecular H-bonds ranges from 2.5 to 14.0 kcal/mol [31]. In the 1,3-propanediol/H₂O system, the calculated energy of H-bonds between water molecules (Figure 4a) was 20.48 kJ/mol, and the energy of the H-bond between 1,3-propanediol molecules (Figure 4d) was 32.31 kJ/mol (Table 1). However, the energy of the H-bond between 1,3-propanediol and BA reached 40.16 kJ/mol, and the total intermolecular force was 72.38 kJ/mol (Table 1). The strength of the H-bond between 1,3-propanediol and BA is stronger than that of the H-bond between 1,3-propanediol and 1,3-propanediol. In addition, the H-bond energy between two 1,3-propanediol molecules and one BA molecule was also simulated, indicating that the biggest energy of the H-bond between 1,3-propanediol and BA reached 43.55 kJ/mol. It was thus predicted that the intermolecular force between PVA and BA should be greater than that between PVA and PVA, which might account for the improvement of PVA/BA films. The elongation at break of PVA/BA films is also increased by this physical improve-

ment, in contrast to the chemical cross-linking, which reduces elongation at break. The hypothesized physical cross-linking network of H-bonds between PVA and BA was based on the outcomes of IR and Gaussian simulations (Figure 5). Due to the interaction of the H-bonds, BA is thought of as a reinforcing agent to enhance both the tensile strength and elongation at break.

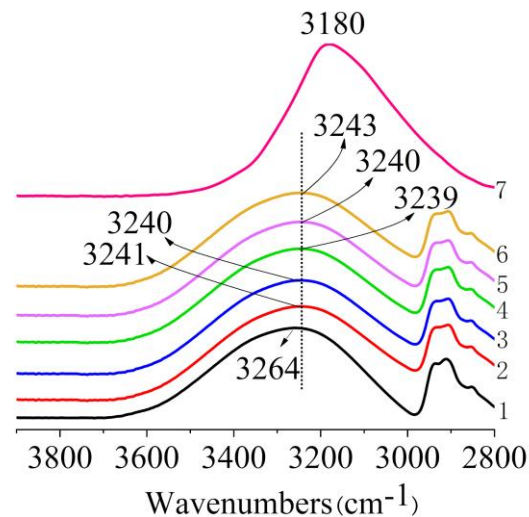


Figure 3. FTIR spectra of BA, PVA, and PVA/BA films of 2800–3900 cm^{-1} . (1) PVA, (2) PVA-0.1 wt%, (3) PVA-0.3 wt%, (4) PVA-0.5 wt%, (5) PVA-0.8 wt%, (6) PVA-1.0 wt%, and (7) BA.

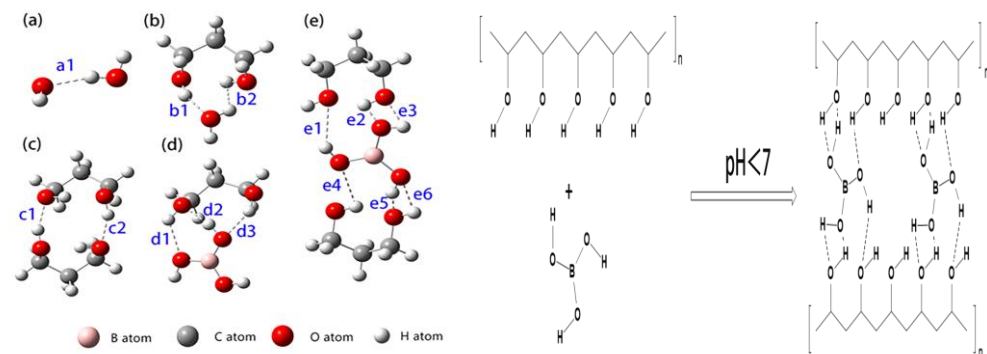


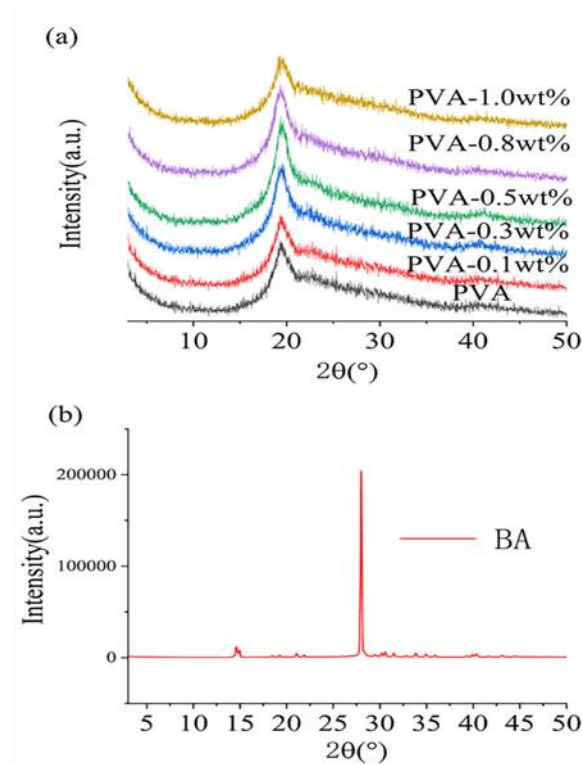
Figure 4. Schemes of H-bonds simulated by Gaussian software. (a) $\text{H}_2\text{O}-\text{H}_2\text{O}$, (b) PVA- H_2O , (c) PVA-PVA, (d) PVA-BA, (e) PVA-BA-PVA, and illustration of hydrogen bonds interaction among PVA and BA.

3.4. Crystallinity of PVA/BA Films

To determine how the mechanical characteristics of PVA/BA films were enhanced, XRD analysis may be performed. The X-ray diffraction patterns of pure BA, PVA, and various PVA/BA composite films are shown in Figure 5. The neat PVA's diffraction peaks, which are centered at $2\theta = 19.6^\circ$, serve as a representation of the (101) plane of PVA crystals. A particular crystal is BA (Figure 5b). The PVA diffraction peaks in PVA/BA films did not move when BA was added, indicating that the crystal had not changed in any way. However, as BA concentration rose to 0.5 wt percent of BA, the regions of diffraction peaks at $2\theta = 19.6^\circ$ steadily grew before declining in the opposite direction as BA content rose. Consequently, crystallinity peaked when BA content reached 0.5 wt%.

Table 1. H-bond length and energy of the intermolecular interaction of H₂O-H₂O, PVA-H₂O, PVA-BA, PVA-PVA, and PVA-BA-PVA calculated by the Gaussian simulation.

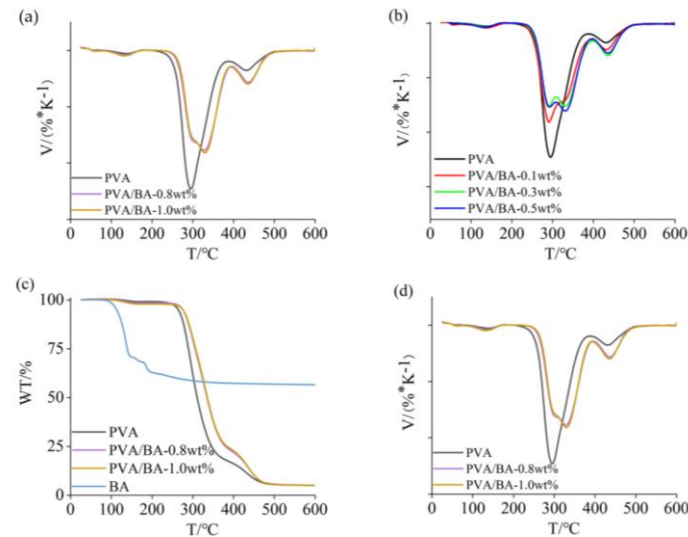
H ₂ O-H ₂ O			PVA-H ₂ O			PVA-PVA		
	Length	Energy (kJ/mol)		Length	Energy (kJ/mol)		Length	Energy (kJ/mol)
a1	1.91	20.48	b1	1.84	28.13	c1	1.78	32.31
			b2	1.84	28.13	c2	1.78	32.31
PVA-BA			PVA-BA-PVA					
	Length	Energy (kJ/mol)		Length	Energy (kJ/mol)		Length	Energy (kJ/mol)
d1	2.16	11.82	e1	2.41	9.43	e4	2.41	9.45
d2	1.71	40.16	e2	1.61	43.55	e5	1.61	43.52
d3	1.92	20.40	e3	1.83	24.87	e6	1.83	24.86

**Figure 5.** (a) X-ray diffraction of PVA and PVA/BA composite films with various BA contents, (b) X-ray diffraction of BA.

3.5. Thermal Properties of Films

To evaluate the effect of BA and H-bonds on the thermal properties of PVA, DSC, and TGA were utilized. Figure 6 displays the TGA and DTG curves for BA, PVA, and PVA/BA films. The data are summarized below in the figure. Peak temperatures for PVA film thermal breakdown were 297 °C (T_{max1}) and 430 °C (T_{max2}). The elimination of hydroxyl groups from the side chain and the disintegration of the main chain should happen at 297 °C and 430 °C, respectively. The PVA film's initial breakdown temperature (T_i) is 242 °C. T_i of the PVA/BA film tended to rise with the addition of BA, reaching a maximum of 268 °C at 1.0 wt% BA, which is 26 °C higher than that of PVA. T_{max1} was divided into two peaks (DTG curves), whether the BA concentration was 0.3 wt% or 0.5 wt%, suggesting a shift in the structure of the films. The T_{max1} became one peak once again at a temperature that was 30 °C higher than 297 °C when the BA concentration was

over 0.8 wt%, suggesting that the PVA/BA films should be more stable. Tmax2 of PVA/BA films did not substantially differ from Tmax2 of PVA film, indicating that the main chain's structural integrity was unaffected.



TGA data

Samples	T _i / °C	T _{max1} / °C	T _{max2} / °C	Final residual Weight/%
PVA	242	297/-	430	2.4
PVA-0.1 wt%	245	292/-	431	3.1
PVA-0.3 wt%	252	289/329	430	3.4
PVA-0.5 wt%	257	290/330	435	3.6
PVA-0.8 wt%	264	-/328	434	3.7
PVA-1.0 wt%	268	-/330	435	3.6
BA	193	-	-	52.6

DTG data

Samples	PVA (wt%)	BA (wt%)	T _m (°C)	ΔH _m (J/g)	χ _c (%)
PVA	100.0	0	220.3	48.3	34.8
PVA-0.1 wt%BA	99.9	0.1	219.6	50.2	36.2
PVA-0.3 wt%BA	99.7	0.3	218.1	51.3	37.0
PVA-0.5 wt%BA	99.5	0.5	217.4	54.4	39.2
PVA-0.8 wt%BA	99.2	0.8	215.3	50.7	36.6
PVA-1.0 wt%BA	99.0	1.0	213.7	49.8	35.9

Figure 6. TGA (a,c) and DTG (b,d) curves of BA, PVA, and PVA/BA films and their summarized data (Tables).

The last table below the figure summarizes the DSC data. Pure PVA has a melting point (T_m) of 220.3 °C and a degree of crystallinity (c) of 34.8 percent based on 138.6 J/g of melting enthalpy (H_{m0}) of 100% crystalline PVA. As the BA concentration increased, the crystallinity rose, then fell once the BA level rose above 0.5 weight percent. A maximum crystallinity was observed at 0.5 weight percent BA, according to the XRD data. In addition, X-ray diffraction (XRD) patterns or relative crystallinity decrease with increasing concentration of added materials that interact with the starting material [39].

Although the contents of BA were within 1.0 wt%, BA still had significantly positive effects on the thermal stability and crystallinity of PVA/BA composite films.

3.6. Surface and Cross-Section Morphologies of PVA and PVA/BA Films

The surfaces and cross-sections of the PVA and PVA/BA films are shown in SEM pictures in Figure 7. PVA/BA films have very smooth surfaces with a surface morphology that is comparable to that of pure PVA films. PVA and PVA/BA film cross-sections were likewise in the same, consistent condition. It suggested that PVA and BA worked well together.

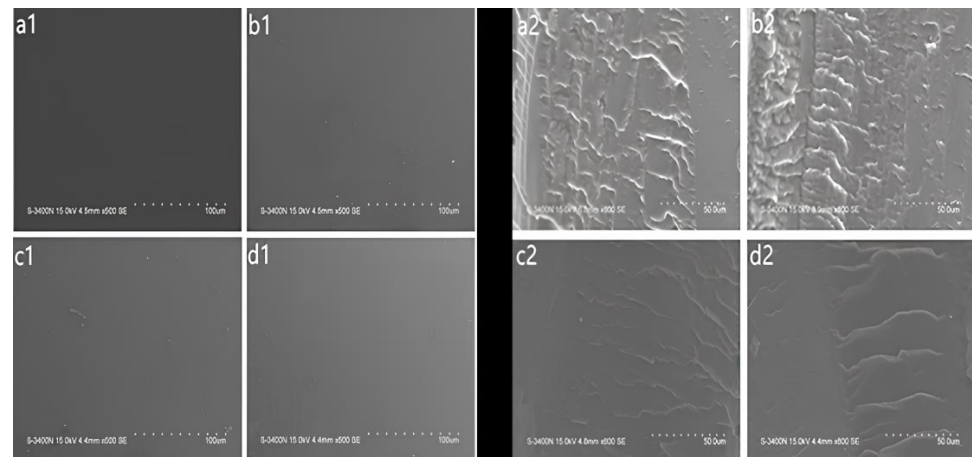


Figure 7. SEM images of films for surfaces (a1,b1,c1,d1) and cross-sections (a2,b2,c2,d2). (a1,a2) pure PVA film, (b1,b2) PVA-0.1 wt%, (c1,c2) PVA-0.3 wt%, and (d1,d2) PVA-0.5 wt%.

3.7. Antimicrobial Properties of PVA/BA/PHMG Films

Since infections caused by pathogenic and resistant bacteria continue to endanger public health, the evaluation and production of antibacterial films, especially against them, are still of interest to scientists [40]. Figure 8 displays the antibacterial graphs of PVA/BA/PHMG and pure PVA film. Significant bacterial growth is seen in Figure 8's panels a1 and b1, demonstrating that the pure PVA film had no antibacterial effect on *E. coli* and *S. aureus*. Figure 8(a2,b2) show the test results for the PVA/BA/PHMG-0.1 wt% film against *E. coli* and *S. aureus*. No bacterial growth was seen on the PVA/BA/PHMG-0.1 wt% film in the Petri dishes.

Table 2 shows the results of bacterial inhibition rates of pure PVA films and PVA/BA/PHMG films after water washing. The PVA film and PVA/BA film had no antibacterial properties, while the PVA/BA/PHMG films achieved 99.99% antibacterial rates even after ten cycles of water washing. This indicates that the PHMG is non-leaching.

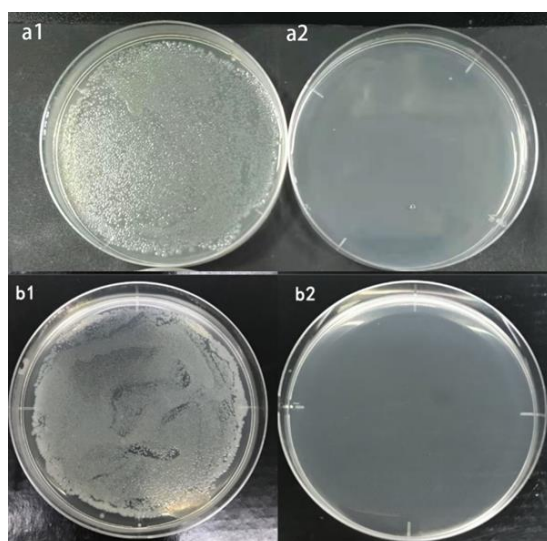


Figure 8. Antimicrobial photos of pure PVA film against *E. coli* (a1) and against *S. aureus* (b1). Antimicrobial photos of PVA/BA/PHMG-0.5 wt% film against *E. coli* (a2) and against *S. aureus* (b2) after 10 cycles of DI water washing.

Table 2. Antimicrobial rates of PVA/BA/PHMG films after washing with DI water.

Samples	Antimicrobial Rates against <i>E. coli</i> (%)				Antimicrobial Rates against <i>S. aureus</i> (%)			
	Before Washing	Cycles of Water Washing			Before Washing	Cycles of Water Washing		
		1	5	10		1	5	10
Neat PVA	0	0	0	0	0	0	0	0
PVA/BA-0.5 wt%	0	0	0	0	0	0	0	0
PVA/BA/PHMG-0.1 wt%	99.99	99.99	99.99	99.99	99.99	99.99	99.99	99.99
PVA/BA/PHMG-0.5 wt%	99.99	99.99	99.99	99.99	99.99	99.99	99.99	99.99
PVA/BA/PHMG-1.0 wt%	99.99	99.99	99.99	99.99	99.99	99.99	99.99	99.99

4. Conclusions

Novel bioactive materials based on poly(vinyl alcohol) (PVA)/BA and PVA/BA/PHMG were successfully synthesized and characterized using X-ray and FTIR techniques. The components were found to be compatible and interacted through hydrogen bonds. The mechanical analysis showed that PHMG acted as a plasticizer, increasing the elasticity of the materials. Similarly, the films containing PVA/PHMG exhibited enhanced bactericidal properties. Introducing poly(hexamethylene guanidine) or PHMG into PVA and PVA/BA mixture improved the thermal stability, attributed to the nitrogen atoms hindering oxygen diffusion. The PHMG also played a role as a dye, as evident from color changes. Surface analysis revealed that PVA/BA films had smoother surfaces due to strong hydrogen bonding, while the addition of PHMG increased hydrophilicity and reduced bacterial adhesion. The PVA/BA and PVA/BA/PHMG films in this investigation were strengthened and transparent via solution casting. Elongation at break and tensile strength of PVA/BA films increased by 46 and 70 percent, respectively. These changes were mainly brought about by the formation of an H-bond between PVA and BA. PVA, BA, and PHMG films have exceptional mechanical properties and broad-spectrum antibacterial properties (antimicrobial rates against *Escherichia coli* and *Staphylococcus aureus* more than 99.99 percent). This simple, eco-friendly preparation offers a useful way to produce PVA films that are strong, non-leaching, and antibacterial.

Author Contributions: Conceptualization: D.W., X.X. and Y.G.; Methodology: D.W.; Software: D.W.; Validation: D.W., X.X. and Y.G.; Formal analysis: S.Z.; Investigation: S.Z.; Resources: S.Z.; Data curation: D.W.; Writing—original draft preparation: S.Z.; Writing—review and editing: D.W.; Visualization: D.W.; supervision: D.W. All authors have read and agreed to the published version of the manuscript.

Funding: This research received no external funding.

Institutional Review Board Statement: Not applicable.

Informed Consent Statement: Not applicable.

Data Availability Statement: Not applicable.

Conflicts of Interest: The authors declare no conflict of interest.

References

1. Abdullah, Z.W.; Dong, Y.; Davies, I.J.; Barbhuiya, S. PVA, PVA Blends, and Their Nanocomposites for Biodegradable Packaging Application. *Polym.-Plast. Technol. Eng.* **2017**, *56*, 1307–1344. [[CrossRef](#)]
2. Zhao, G.; Shi, L.; Yang, G.; Zhuang, X.; Cheng, B. 3D fibrous aerogels from 1D polymer nanofibers for energy and environmental applications. *J. Mater. Chem. A* **2023**, *11*, 512–547. [[CrossRef](#)]
3. Abrial, H.; Atmajaya, A.; Mahardika, M.; Hafizulhaq, F.; Kadriadi; Handayani, D.; Sapuan, S.M.; Ilyas, R.A. Effect of ultrasonication duration of polyvinyl alcohol (PVA) gel on characterizations of PVA film. *J. Mater. Res. Technol.* **2020**, *9*, 2477–2486. [[CrossRef](#)]
4. Olewnik-Kruszkowska, E.; Gierszewska, M.; Jakubowska, E.; Tarach, I.; Sedlarik, V.; Pummerova, M. Antibacterial Films Based on PVA and PVA-Chitosan Modified with Poly(Hexamethylene Guanidine). *Polymers* **2019**, *11*, 2093. [[CrossRef](#)]
5. Kochkina, N.E.; Lukin, N.D. Structure and properties of biodegradable maize starch/chitosan composite films as affected by PVA additions. *Int. J. Biol. Macromol.* **2020**, *157*, 377–384. [[CrossRef](#)]
6. Chen, K.; Liu, J.; Yang, X.; Zhang, D. Preparation, optimization and property of PVA-HA/PAA composite hydrogel. *Mater. Sci. Eng. C Mater. Biol. Appl.* **2017**, *78*, 520–529. [[CrossRef](#)]
7. Leone, G.; Consumi, M.; Lamponi, S.; Bonechi, C.; Tamasi, G.; Donati, A.; Rossi, C.; Magnani, A. Thixotropic PVA hydrogel enclosing a hydrophilic PVP core as nucleus pulposus substitute. *Mater. Sci. Eng. C Mater. Biol. Appl.* **2019**, *98*, 696–704. [[CrossRef](#)] [[PubMed](#)]
8. Wu, X.; Xie, Y.; Xue, C.; Chen, K.; Yang, X.; Xu, L.; Qi, J.; Zhang, D. Preparation of PVA-GO composite hydrogel and effect of ionic coordination on its properties. *Mater. Res. Express* **2019**, *6*, 075306. [[CrossRef](#)]
9. Chen, Y.; Li, J.; Lu, J.; Ding, M.; Chen, Y. Synthesis and properties of Poly(vinyl alcohol) hydrogels with high strength and toughness. *Polym. Test.* **2022**, *108*, 107516. [[CrossRef](#)]
10. Cao, M.; Liu, Z.; Xie, C. Effect of steel-PVA hybrid fibers on compressive behavior of CaCO₃ whiskers reinforced cement mortar. *J. Build. Eng.* **2020**, *31*, 101314. [[CrossRef](#)]
11. Assaedi, H.; Alomayri, T.; Siddika, A.; Shaikh, F.; Alamri, H.; Subaer, S.; Low, I.M. Effect of Nanosilica on Mechanical Properties and Microstructure of PVA Fiber-Reinforced Geopolymer Composite (PVA-FRGC). *Materials* **2019**, *12*, 3624. [[CrossRef](#)]
12. Piacentini, E.; Bazzarelli, F.; Poerio, T.; Albisa, A.; Irusta, S.; Mendoza, G.; Sebastian, V.; Giorno, L. Encapsulation of water-soluble drugs in Poly (vinyl alcohol) (PVA)- microparticles via membrane emulsification: Influence of process and formulation parameters on structural and functional properties. *Mater. Today Commun.* **2020**, *24*, 100967. [[CrossRef](#)]
13. Wang, L.; Ding, Y.; Li, N.; Chai, Y.; Li, Q.; Du, Y.; Hong, Z.; Ou, L. Nanobody-based polyvinyl alcohol beads as antifouling adsorbents for selective removal of tumor necrosis factor-alpha. *Chin. Chem. Lett.* **2022**, *33*, 2512–2516. [[CrossRef](#)]
14. Abdullah, Z.W.; Dong, Y.; Han, N.; Liu, S. Water and gas barrier properties of polyvinyl alcohol (PVA)/starch (ST)/ glycerol (GL)/halloysite nanotube (HNT) bionanocomposite films: Experimental characterisation and modelling approach. *Compos. Part B Eng.* **2019**, *174*, 107033. [[CrossRef](#)]
15. Kim, J.M.; Lee, M.H.; Ko, J.A.; Kang, D.H.; Bae, H.; Park, H.J. Influence of Food with High Moisture Content on Oxygen Barrier Property of Polyvinyl Alcohol (PVA)/Vermiculite Nanocomposite Coated Multilayer Packaging Film. *J. Food Sci.* **2018**, *83*, 349–357. [[CrossRef](#)]
16. Virly; Chiu, C.H.; Tsai, T.Y.; Yeh, Y.C.; Wang, R. Encapsulation of beta-Glucosidase within PVA Fibers by CCD-RSM-Guided Coelectrospinning: A Novel Approach for Specific Mogroside Sweetener Production. *J. Agric. Food Chem.* **2020**, *68*, 11790–11801. [[CrossRef](#)]
17. Mallakpour, S.; Darvishzadeh, M. Ultrasonic treatment as recent and environmentally friendly route for the synthesis and characterization of polymer nanocomposite having PVA and biosafe BSA-modified ZnO nanoparticles. *Polym. Adv. Technol.* **2018**, *29*, 2174–2183. [[CrossRef](#)]
18. Suganthi, S.; Vignesh, S.; Kalyana Sundar, J.; Raj, V. Fabrication of PVA polymer films with improved antibacterial activity by fine-tuning via organic acids for food packaging applications. *Appl. Water Sci.* **2020**, *10*, 100. [[CrossRef](#)]

19. Silva, G.G.D.; Sobral, P.J.A.; Carvalho, R.A.; Bergo, P.V.A.; Mendieta-Taboada, O.; Habitante, A.M.Q.B. Biodegradable Films Based on Blends of Gelatin and Poly (Vinyl Alcohol): Effect of PVA Type or Concentration on Some Physical Properties of Films. *J. Polym. Environ.* **2008**, *16*, 276–285. [[CrossRef](#)]
20. Zain, N.A.M.; Suhaimi, M.S.; Idris, A. Development and modification of PVA–alginate as a suitable immobilization matrix. *Process Biochem.* **2011**, *46*, 2122–2129. [[CrossRef](#)]
21. Mahmood, R.S.; Salman, S.A.; Bakr, N.A. The electrical and mechanical properties of Cadmium chloride reinforced PVA:PVP blend films. *Pap. Phys.* **2020**, *12*. [[CrossRef](#)]
22. Zhu, H.; Cao, H.; Liu, X.; Wang, M.; Meng, X.; Zhou, Q.; Xu, L. Nacre-like composite films with a conductive interconnected network consisting of graphene oxide, polyvinyl alcohol and single-walled carbon nanotubes. *Mater. Des.* **2019**, *175*, 107783. [[CrossRef](#)]
23. Fan, L.; Zhang, H.; Gao, M.; Zhang, M.; Liu, P.; Liu, X. Cellulose nanocrystals/silver nanoparticles: In-situ preparation and application in PVA films. *Holzforchung* **2020**, *74*, 523–528. [[CrossRef](#)]
24. Yao, K.; Cai, J.; Liu, M.; Yu, Y.; Xiong, H.; Tang, S.; Ding, S. Structure and properties of starch/PVA/nano-SiO₂ hybrid films. *Carbohydr. Polym.* **2011**, *86*, 1784–1789. [[CrossRef](#)]
25. Sabourian, P.; Frounchi, M.; Dadbin, S. Polyvinyl alcohol and polyvinyl alcohol/ polyvinyl pyrrolidone biomedical foams crosslinked by gamma irradiation. *J. Cell. Plast.* **2016**, *53*, 359–372. [[CrossRef](#)]
26. Chen, J.; Li, Y.; Zhang, Y.; Zhu, Y. Preparation and characterization of graphene oxide reinforced PVA film with boric acid as crosslinker. *J. Appl. Polym. Sci.* **2015**, *132*, 42000. [[CrossRef](#)]
27. Cao, W.; Yue, L.; Wang, Z. High antibacterial activity of chitosan—Molybdenum disulfide nanocomposite. *Carbohydr. Polym.* **2019**, *215*, 226–234. [[CrossRef](#)] [[PubMed](#)]
28. Lu, J.; Chen, Y.; Ding, M.; Fan, X.; Hu, J.; Chen, Y.; Li, J.; Li, Z.; Liu, W. A 4arm-PEG macromolecule crosslinked chitosan hydrogels as antibacterial wound dressing. *Carbohydr. Polym.* **2022**, *277*, 118871. [[CrossRef](#)]
29. Ma, W.; Li, L.; Liu, Y.; Sun, Y.; Kim, I.S.; Ren, X. Tailored assembly of vinylbenzyl N-halamine with end-activated ZnO to form hybrid nanoparticles for quick antibacterial response and enhanced UV stability. *J. Alloys Compd.* **2019**, *797*, 692–701. [[CrossRef](#)]
30. Xiong, K.-R.; Liang, Y.-R.; Ou-yang, Y.; Wu, D.-C.; Fu, R.-W. Nanohybrids of silver nanoparticles grown in-situ on a graphene oxide silver ion salt: Simple synthesis and their enhanced antibacterial activity. *Carbon* **2020**, *158*, 426–433. [[CrossRef](#)]
31. Liu, M.; Wang, F.; Liang, M.; Si, Y.; Yu, J.; Ding, B. In situ green synthesis of rechargeable antibacterial N-halamine grafted poly(vinyl alcohol) nanofibrous membranes for food packaging applications. *Compos. Commun.* **2020**, *17*, 147–153. [[CrossRef](#)]
32. Guo, C.; Zhang, J.; Feng, X.; Du, Z.; Jiang, Y.; Shi, Y.; Yang, G.; Tan, L. Polyhexamethylene biguanide chemically modified cotton with desirable hemostatic, inflammation-reducing, intrinsic antibacterial property for infected wound healing. *Chin. Chem. Lett.* **2022**, *33*, 2975–2981. [[CrossRef](#)]
33. Li, Y.; Zheng, H.; Liang, Y.; Xuan, M.; Liu, G.; Xie, H. Hyaluronic acid-methacrylic anhydride/polyhexamethylene biguanide hybrid hydrogel with antibacterial and proangiogenic functions for diabetic wound repair. *Chin. Chem. Lett.* **2022**, *33*, 5030–5034. [[CrossRef](#)]
34. Wei, D.; Ma, Q.; Guan, Y.; Hu, F.; Zheng, A.; Zhang, X.; Teng, Z.; Jiang, H. Structural characterization and antibacterial activity of oligoguanidine (polyhexamethylene guanidine hydrochloride). *Mater. Sci. Eng. C* **2009**, *29*, 1776–1780. [[CrossRef](#)]
35. Abedinia, A.; Ariffin, F.; Huda, N.; Nafchi, A.M. Preparation and characterization of a novel biocomposite based on duck feet gelatin as alternative to bovine gelatin. *Int. J. Biol. Macromol.* **2018**, *1*, 855–862. [[CrossRef](#)] [[PubMed](#)]
36. Patil, A.S.; Waghmare, R.D.; Pawar, S.P.; Salunkhe, S.T.; Kolekar, G.B.; Sohn, D.; Gore, A.H. Photophysical insights of highly transparent, flexible and re-emissive PVA @ WTR-CDs composite thin films: A next generation food packaging material for UV blocking applications. *J. Photochem. Photobiol. A Chem.* **2020**, *400*, 112647. [[CrossRef](#)]
37. Wei, D.; Zhou, R.; Guan, Y.; Zheng, A.; Zhang, Y. Investigation on the reaction between polyhexamethylene guanidine hydrochloride oligomer and glycidyl methacrylate. *J. Appl. Polym. Sci.* **2013**, *127*, 666–674. [[CrossRef](#)]
38. Emamian, S.; Lu, T.; Kruse, H.; Emamian, H. Exploring Nature and Predicting Strength of Hydrogen Bonds: A Correlation Analysis Between Atoms-in-Molecules Descriptors, Binding Energies, and Energy Components of Symmetry-Adapted Perturbation Theory. *J. Comput. Chem.* **2019**, *40*, 2868–2881. [[CrossRef](#)]
39. Tarahi, M.; Hedayati, S.; Shahidi, F. Effects of mung bean (*Vigna radiata*) protein isolate on rheological, textural, and structural properties of native corn starch. *Polymers* **2022**, *14*, 3012. [[CrossRef](#)]
40. Yang, R.; Hou, E.; Cheng, W.; Yan, X.; Zhang, T.; Li, S.; Yao, H.; Liu, J.; Guo, Y. Membrane-Targeting Neolignan-Antimicrobial Peptide Mimic Conjugates to Combat Methicillin-Resistant *Staphylococcus aureus* (MRSA) Infections. *J. Med. Chem.* **2022**, *65*, 16879–16892. [[CrossRef](#)]

Disclaimer/Publisher’s Note: The statements, opinions and data contained in all publications are solely those of the individual author(s) and contributor(s) and not of MDPI and/or the editor(s). MDPI and/or the editor(s) disclaim responsibility for any injury to people or property resulting from any ideas, methods, instructions or products referred to in the content.